Chapter 1
Introduction

How unique is the solar system? Until relatively recently, the solar system was the only example of a planetary system we knew, and the concept of planets in distant regions of the galaxy belonged to the realm of science fiction. While the sheer number of stars in the universe hinted that our eight planets might not be an exception to the rule, we did not have any confirmation of the existence of other planets, or any clues of how these systems could look like. Until the late 20th Century, the solar system was most certainly unique, at least to the best of our knowledge.

Since the first discovery of a planet orbiting a Sun-like star in 1995 (Mayor & Queloz, 1995), observational surveys have revealed an incredible variety of planetary systems. As of October 2020, 4370 planets[1] around stars other than the Sun, or exoplanets, have been detected. Somewhat surprisingly, the discovery of so many new planetary systems has not made our own look any less unique. If there is one thing that all planetary systems seem to have in common is their unlikeness.
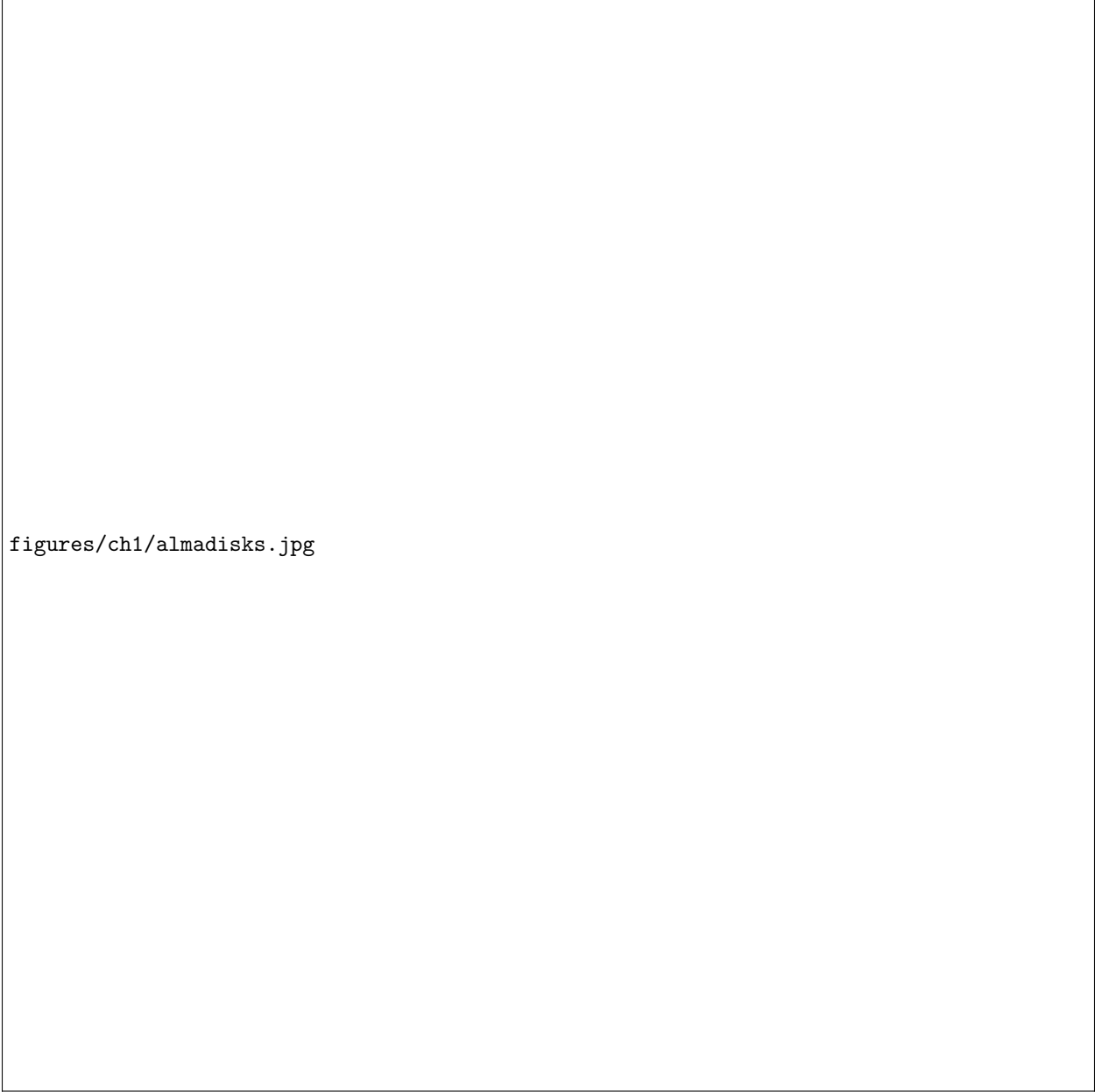
The current image we have of star and planet formation has its origins in the 18th Century, in particular in the nebular hypothesis first developed by French polymath and mathematician Pierre-Simon Laplace, and German philosopher Immanuel Kant. The premise was simple: Kant (1755) conjectured that the back then newly-observed nebulae (e.g. Halley, 1715) were locations of star and planet formation. A similar conclusion was reached independently by Laplace (1796), who also argued that it was the collapse of these nebulae which brought on the formation of a star, along with the material around it forming the shape of a disk. It was not until 1978 when this premise surfaced again in the work of Prentice (1978). The first detection of a circumstellar disk, around the star β Pictoris, was reported in Smith & Terrile (1984).

The first observations of resolved circumstellar disks were in the Orion nebula, where their dark silhouettes against the bright nebulous background were imaged by the Hubble Space Telescope (O'dell & Wen, 1994). Nowadays, modern telescopes such as the Very Large Telescope (VLT) and the Atacama Large Millimetre/submillimeter Array (ALMA), both located in the magnificently beautiful Atacama desert in the north of Chile, have opened our eyes to the detailed substructure of these disks, allowing us to see planet formation as it happens.

Further observations of circumstellar disk populations suggest that the environment in which they are immersed can have important repercussions for their potential to form planets. If planets do eventually form, their composition and dynamical configurations are likely to be shaped by the surroundings of their original disks. To answer the question of how unique the solar system is, we then have to take a step back in time, and look not just at the current configuration of our home system, but also at the conditions during its formation.

This thesis looks to quantify the effects that the star formation environment has over the young circumstellar disks. To do this, we perform numerical simulations of circumstellar disks which are affected by several ambient mechanisms that have been observed in star forming regions. We look to determine how these processes influence the mass reservoir of the disks, and how they constrain their potential to form planets. In the following Sections of this Chapter we set the scientific context for this work. In Section 5 we outline the goals and following Chapters of the thesis.

---

[1]Data from `http://exoplanet.eu`, last accessed on 31 October 2020

Figure 1: A sample of disks from ALMA's highest resolution survey, the Disc Substructures at High Angular Resolution Project (DSHARP). *ALMA (ESO/NAOJ/NRAO), S. Andrews et al.; NRAO/AUI/NSF, S. Dagnello.*

1 Star clusters

Star clusters are studied from many different areas in astrophysics. Beyond being of interest for their inner stellar dynamics and stellar evolution processes, star clusters are probes for star formation in distant galaxies and can provide insights into galaxy assembly (see Kruijssen, 2014; Forbes et al., 2018, for recent reviews on this topic). In this thesis we focus our interest in star clusters as the birth sites of stars and circumstellar disks.

There is not a single definition of star cluster. Portegies Zwart et al. (2010) define a star cluster simply as a group stars which are gravitationally bound. According to Lada & Lada (2003) star clusters are defined as groups of stars which are gravitationally bound and whose stellar mass density is enough to keep the conglomerate stable against the tidal field of the galaxy and passing interstellar clouds, assuming virial equilibrium. Adams & Myers (2001) propose an additional criterion that the number of stars in the cluster is enough so that it does not evaporate in 10^8 Gyr, which is typical lifetime of open clusters in the field. Krumholz & McKee (2020) follow the simple definition of Trumpler (1930) and define star clusters as stellar groups which are not dominated by dark matter (separating them from galaxies) and with a mean stellar density that is at least a few times higher than the background. This allows to define star clusters very generally and remarks the fact that, while different types of clusters exist (see below), their dynamics and evolution are similar. There is no evidence that the different types of star clusters actually form differently (Elmegreen & Efremov, 1997; Krumholz & McKee, 2020).

Stars clusters are generally divided into three broad categories: globular clusters, open clusters, and associations. Globular clusters are generally massive ($M_c \gtrsim 10^5$ $M_\odot$) and old ($\gtrsim 10$ Gyr), containing hundreds of thousands of stars (Portegies Zwart et al., 2010). Open clusters are younger ($\lesssim 0.3$ Gyr) and less massive ($M_c \lesssim 10^3$ $M_\odot$), and generally contain a few hundred stars. Stellar associations are unbound conglomerates with a less than a hundred stars (Adams & Myers, 2001; Gieles & Portegies Zwart, 2011).

1.1 Formation and evolution

Stars form from the collapse of a giant molecular cloud. These clouds are located in large complexes in the spiral arms of galaxies. The masses of individual clouds can go up to 10^6 $M_\odot$ and sizes up to 100 pc (Larson, 2003). These clouds are not homogeneous in density, and they present substructure in the form of clumps and filaments arranged in a partly hierarchical fashion which can be approximated with fractal models (e.g. Scalo, 1990; Elmegreen & Falgarone, 1996; Elmegreen et al., 2000; Williams et al., 2000; Bate, 2010; Hacar et al., 2013; Chevance et al., 2020; Krause et al., 2020). These clumps have masses ranging from ~ 1 $M_\odot$ to several thousand solar masses, and sizes from 0.1 pc to several parsec (Larson, 2003). The irregular shapes of the clouds and their substructure suggest that these arrangements might be modelled by turbulent flows (Falgarone et al., 1991; Falgarone & Phillips, 1991).

Depending on their mass, the clumps within giant molecular clouds can form individual stars, small multiple systems, or large star clusters (e.g. Lada et al., 1993; Larson, 1995; Williams et al., 2000; Lada & Lada, 2003; Bate, 2012). The star formation process remains the same across these different scales, and it begins with the collapse of a clump. Regardless of their substructure, molecular clouds have typical temperatures of $\sim 10 - 20$ K across their range of different densities (e.g. Larson, 1985; Masunaga & Inutsuka, 2000). The combination of low, constant temperature and high densities in the clumps make them Jeans unstable (Jeans, 1902), meaning that a small gravitational instability can grow exponentially and cause the clump to fragment into smaller and smaller pieces in a chain reaction-like effect. The fragmentation will continue as long as the gas can cool efficiently (e.g. Hoyle, 1953; Hunter, 1964, 1977; Field et al., 2008; Vázquez-Semadeni et al., 2019).

As the fragmentation continues, some of the smallest pieces will reach densities high enough to form a star. This point-like source will be surrounded by an envelope of infalling material. These high density points, which can now be referred to as protostars, have initial masses $\sim 10^{-2}$ $M_\odot$ and will continue growing by accreting material from the envelope (e.g. Larson, 1969; Appenzeller & Tscharnuter, 1975; Winkler & Newman, 1980; Masunaga & Inutsuka, 2000; Wuchterl & Tscharnuter, 2003). It is at this moment when circumstellar disks begin to form. In the present section we will continue describing the star cluster formation process, and resume describing disk formation in Section 2.1.

The total angular momentum in a giant molecular cloud is too large to be contained in a single star (e.g.

Mestel & Spitzer, 1956; Mestel, 1965; Spitzer, 1968; Bodenheimer et al., 2000). As such, the fragmentation process results not only in the formation of individual stars, but also in stellar aggregates. The substructure present in the clouds plays an important role in establishing the kinematics and structure of young clusters (e.g. Klessen et al., 2000; Klessen & Burkert, 2000; Kruijssen et al., 2012).

There are two main scenarios of star cluster formation: *in-situ* formation and conveyor belt formation (e.g. Longmore et al., 2014; Krumholz & McKee, 2020). The differences between the two concern mostly the extent of the initial gas compared with the radius of the final cluster. *In-situ* formation refers to the cluster forming rapidly from a clump or cloud of gas. The size of the initial gas cloud will be the same as the final radius of the cluster. This mechanism requires for star formation to happen very quickly, in about one dynamical timescale (see Section 1.2) (Longmore et al., 2014). The conveyor belt scenario considers the initial gas to be much more extended than the final cluster, probably by several cluster radii. The clumps and filaments present in the cloud accrete gas from the outer regions and direct it to the protostars.

Regardless of the formation scenario, the young stellar clusters are still embedded in leftover gas. In an ideal system, all the gas in the molecular cloud would turn into stars. However, several mechanisms that arise from the star formation process itself can reduce the amount of gas available to form stars. Protostellar outflows (e.g. Matzner & McKee, 2000; Bally, 2016; Offner & Chaban, 2017), photoionization feedback (e.g. Williams & McKee, 1997; Matzner, 2002; Murray & Rahman, 2010), radiation pressure (e.g. Fall et al., 2010; Murray & Rahman, 2010; Grudić et al., 2018), and stellar feedback such as wind and supernovae (e.g. Vink et al., 2001; Pelupessy & Portegies Zwart, 2012; Offner & Arce, 2015) can all reduce the amount of gas available for star formation. To form bound clusters, $\sim 30\%$ to 50% of the gas must be turned into stars before feedback mechanisms begin (Lada et al., 1984; Goodwin, 1997; Clarke et al., 2000). During the embedded stage the stars in the clusters are only visible in infrared wavelengths (Figure 2).

In young star clusters, 50% to 90% of the total mass can be comprised of leftover gas (e.g. Lada & Lada, 1991; Clarke et al., 2000), whereas it is not present in older systems (e.g. Lada & Lada, 1995; Portegies Zwart et al., 2010). The removal of the leftover gas has important consequences in the dynamics of the cluster. In particular, the initial gas fraction and the rate at which the gas is expelled are important. Losing $\sim 50\%$ of the gas in a short time scale compared with the cluster crossing time (see Section 1.2) results in the cluster becoming unbound (e.g. Clarke et al., 2000; Elmegreen et al., 2000; Portegies Zwart et al., 2010). If the gas expulsion lasts several crossing times, the cluster can adapt to the slow changes in potential and survive as a bound system, keeping most of its stars (e.g. Lada et al., 1984; Baumgardt & Kroupa, 2007; Pelupessy & Portegies Zwart, 2012).

After the gas is completely dispersed from the clusters, their evolution continues to be dominated purely by gravity and stellar evolution. Eventually, clusters lose mass due to both internal and external processes. Stellar evolution causes stars to lose $\sim 20\%$ of their mass in supernova explosions. This mass loss occurs until $\sim 40\,\mathrm{Myr}$ of evolution. These explosions can cause the stellar remnants to escape the cluster, due to the velocity kicks (e.g. Faucher-Giguère & Kaspi, 2006; Kruijssen, 2009). The tidal field of the galaxy can greatly increase mass loss by removing stars from the cluster (e.g. Takahashi & Portegies Zwart, 2000; Baumgardt & Makino, 2003; Lamers et al., 2010). On longer timescales ($t \gtrsim 100\,\mathrm{Myr}$) mass loss is dominated by dynamical relaxation, also known as evaporation or dissolution. This effect is related to the kinetic energy distribution trying to compensate for high-energy stars being kicked out of the cluster. This causes stars to escape the cluster through tidal streams (e.g. Spitzer, 1940; Fujii & Portegies Zwart, 2011; Gnedin et al., 2014; Madrid et al., 2017; Lucas et al., 2018; Dinnbier & Kroupa, 2020). The cluster stars then dissipate into the field.

1.2 Evolutionary time scales and radii

The dynamical evolution of star clusters is studied through a series of time scales and radii. The definitions of these parameters are generally different for theoretical analyses than for observations. This is because several quantities, such as the total mass or the potential energy, are impossible to measure from observations. In this section we deal with theoretical definitions, since these are the ones used in the following chapters of this thesis.

The dynamical time scale, or crossing time, corresponds to the time that it takes for a particle to cross the system and is defined as (Spitzer, 1987):

$$t_{\mathrm{dyn}} = \frac{R_c}{v}, \tag{1}$$
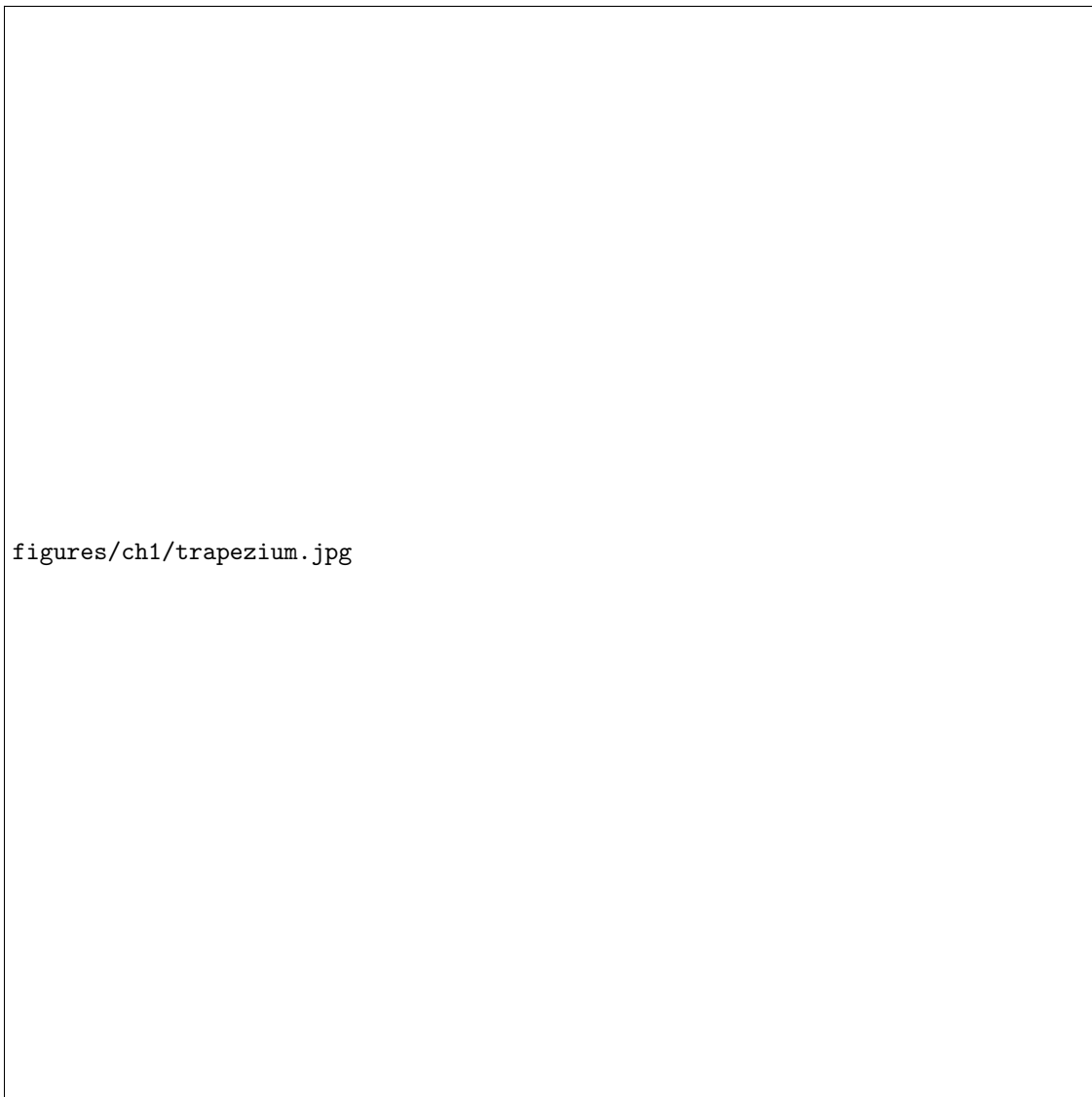
figures/ch1/trapezium.jpg

Figure 2: Trapezium cluster in optical (left) and infrared (right) wavelengths. The stars embedded in the gas are only visible with infrared instruments. *NASA; K.L. Luhman (Harvard-Smithsonian Center for Astrophysics, Cambridge, Mass.); G. Schneider, E. Young, G. Rieke, A. Cotera, H. Chen, M. Rieke, R. Thompson (Steward Observatory, University of Arizona, Tucson, Ariz.); C.R. O'Dell and S.K. Wong (Rice University).*

where R_c is the cluster radius and v is the mean velocity of a star. From the virial theorem, this expression can be rewritten as:

$$t_{\mathrm{dyn}} = \sqrt{\frac{R_c^3}{GM_c}},$$ (2)

where G is the universal gravitational constant and M_c is the mass of the cluster. The dynamical time scale indicates the time in which the system reaches dynamical equilibrium.

Another important time scale is the relaxation time scale. This is the time in which the initial orbits of the stars have been erased by distant interactions with other stars. The relaxation time scale is the time within which global characteristics of the cluster change. It is defined as (Spitzer, 1987):

$$t_{\mathrm{relax}} = \frac{N}{6 \ln(N)} t_{\mathrm{dyn}}.$$ (3)

For a star cluster with $N = 1000$, the relaxation time scale is $t_{\mathrm{relax}} \sim 10\,\mathrm{Myr}$. This is several Myr shorter than the average lifetime of an open cluster. This means that interactions between stars are important during the life of such a cluster and there is significant dynamical evolution. These types of systems are called collisional. On the other hand, a galaxy like the Milky Way ($N \sim 10^{11}$) has a relaxation time scale $t_{\mathrm{relax}} \sim 10^7$ Gyr, so the interactions between stars are not relevant in defining its dynamical evolution. Galaxies are known as collisionless systems.

Star clusters tend to be round and symmetrical, so being able to calculate their radius is useful to follow their evolution. Several definitions of cluster radius exist. The virial radius corresponds to the radius within which the cluster is in virial equilibrium. It is defined as:

$$R_{\mathrm{vir}} = \frac{GM_c^2}{2|U|},$$ (4)

where U is the total potential energy of the system.

The radius of the core of the cluster can be defined theoretically in two ways. When the central density and velocity dispersion are known, the core radius can be defined as (King, 1966):

$$R_{\mathrm{core}} = \sqrt{\frac{3 < v^2 >}{4\pi G \rho}},$$ (5)

where $< v^2 >$ is the velocity dispersion and ρ is the central density. When these values are not easy to obtain, the core radius can be defined using density-weighted nearest neighbours distances (Casertano & Hut, 1985):

$$R_{\mathrm{core}} = \sqrt{\frac{\sum_i \rho_i^2 r_i^2}{\sum_i \rho_i^2}},$$ (6)

where ρ_i is the local number density around star i and r_i is its distance to the k nearest neighbours. In numerical simulations, both definitions of R_{core} behave similarly.

2 Circumstellar disks

Circumstellar disks are a natural outcome of the star formation process. These disks contain the building blocks for future planetary systems. Their different evolutionary paths can help us understand the planet formation process and the diversity of planetary systems we observe today.

Circumstellar disks are geometrically thin (vertical scale height $h << r$) and have masses $M_{\mathrm{disk}} << M_*$. This means that they can be modelled within the theory of thin accretion disks (Pringle, 1981). In particular, they can be described by the similarity solutions for accretion disks by Lynden-Bell & Pringle (1974). In

this frame, the disks are defined by their initial characteristic radius, initial mass, the viscosity at specific radii, and the radial dependence of the viscosity. The characteristic radius of a disk is defined as:

$$R_d(t) = \left(1 + \frac{t}{t_\nu}\right)^{\frac{1}{2-\gamma}} R_c(0), \tag{7}$$

where γ is the radial dependency exponent for the viscosity and t_ν is the viscous time scale of the disk at $t = 0$. The mass of the disk is defined as:

$$M_d(t) = M_d(0) \left(1 + \frac{t}{t_\nu}\right)^{\frac{1}{2\gamma-4}}. \tag{8}$$

The viscous time scale, the time within which angular momentum is redistributed by viscosity, is given by:

$$t_\nu = \frac{R_c(0)}{3(2-\gamma)^2 \nu_c}, \tag{9}$$

where ν_c is the disk viscosity, defined as:

$$\nu_c = \alpha \frac{c_s^2}{\Omega} = \alpha \frac{k_b T \sqrt{R^3}}{\mu m_P \sqrt{GM_*}}. \tag{10}$$

Here, α is the viscosity turbulence parameter (Shakura & Sunyaev, 1973), c_s is the isothermal sound speed, $\Omega = \sqrt{GM/R^3}$ is the keplerian velocity, k_b is the Boltzmann constant, μ is the mean molecular weight of the gas, m_P is the proton mass, T is the disk midplane temperature at R, and M_* is the mass of the host star. Finally, the surface density of the disks is defined by Lynden-Bell & Pringle (1974) as:

$$\Sigma(R, t = 0) = \Sigma_0 \frac{R_c}{R} \exp\left(\frac{-R}{R_c}\right), \tag{11}$$

where R_c is the characteristic radius of the disk as described in Eq. 7, and

$$\Sigma_0 = \frac{M_d}{2\pi R_c^2(1 - \exp(R/Rc))}. \tag{12}$$

The evolution of circumstellar disks is dependent on their viscosity ν_c, which in turn depends on the turbulence parameter α and the radial dependence γ. From Equations 10 and 9 it can be seen that higher values of α result in shorter viscous time scales, meaning rapidly evolving disks. Discs with lower α evolve slower. Values for both parameters have been estimated observationally. Analysing accretion rates in the Taurus and Chamaeleon I molecular cloud complexes, Hartmann et al. (1998) find a value of $\gamma \gtrsim 1$. The limit $\gamma \sim 1$ corresponds to a value of α that is constant all over the disk. With their observed disk sizes, they estimate $\alpha \sim 10^{-2}$. Isella et al. (2009) observe resolved disks in several different regions and find cases for $\gamma > 0$, $\gamma \sim 0$, and even $\gamma < 0$ for some disks. The $\gamma \sim 0$ case corresponds for constant viscosity through the disks. In the disks with $\gamma < 0$ viscosity decreases with radius, which is the opposite of what is expected from the models. They derive values of α ranging from 5×10^{-1} to 10^{-4}. Other surveys have found similar ranges (e.g. Andrews et al., 2010; Mulders & Dominik, 2012; Trapman et al., 2020).

2.1 Formation and evolution

As a direct consequence of angular momentum conservation during the star formation process (Section 1.1), circumstellar disks form within the first 10^4 years after the collapse of a molecular cloud (Yorke et al., 1993; Hueso & Guillot, 2005). While the initial collapse of a clump in a molecular cloud begins into a point source, distant material with higher angular momentum falls inward toward the newly formed protostar (e.g. Bate, 2011). This material will eventually form a disk around the protostar. Initially, the young disk will be surrounded by gas and dust, in what is usually referred to as the embedded stage. At this point, the young star and circumstellar disk are categorised as a Class 0 young stellar object (see Table 1), which have lifetimes $\sim 0.2 \, \text{Myr}$ (Dunham et al., 2015).

Class	Physical properties
0	$M_{env} > M_* > M_{disk}$
I	$M_* > M_{env} \sim M_{disk}$
II	$M_{disk}/M_* \sim 1\%, M_{env} \sim 0$
III	$M_{disk}/M_* << 1\%, M_{env} \sim 0$

Table 1: Classification of young stellar objects. Adapted from Williams & Cieza (2011)

The material which surrounds the disk is accreted into the disk itself or dispersed through outflows and jets (e.g. Elmegreen & Scalo, 2004; Scalo & Elmegreen, 2004; Nakamura & Li, 2012; Bally, 2016). As the envelope starts to dissipate, the system evolves into a Class I object. This stage lasts $\sim 0.5\,\mathrm{Myr}$ (Evans et al., 2009; Williams & Cieza, 2011). The star formation process is effectively over by the end of the Class I phase, and the originally protostellar disk can now be considered protoplanetary. When the dispersal of the envelope is complete and the star at the center of the disk becomes optically visible it is referred to as a Class II object.

The time scales on which disks evolve are too short compared to the lifetime of their host stars. It is not possible to observe ongoing evolutionary processes, and a demographic approach is required to quantify properties of the disks. By observing populations of Class II objects in star forming regions of different ages and densities it is possible to paint a picture of disk evolution.

One of the most important properties of circumstellar disks are their lifetimes, since these set the time available for planet formation. Currently, the best way to estimate disk lifetimes is to measure disk fractions in regions of different ages. The presence of a disk around a star is detected as an infrared excess. The first statistical study of the number of disks in a star forming region was performed by Strom et al. (1989) in Taurus-Auriga. They found that $\sim 80\%$ of stars with ages $\lesssim 1\,\mathrm{Myr}$ have infrared excesses indicating the presence of disks, while less than 10% of stars older that $10\,\mathrm{Myr}$ do. Haisch et al. (2001) study the disk fractions in three star clusters (NGC 2264, NGC 2362, and NGC 1960) and find a half-life $\leq 3\,\mathrm{Myr}$ for the disks, and a mean lifetime of $\sim 6\,\mathrm{Myr}$. From a series of Spitzer Space Telescope surveys, Mamajek (2009) model the decrease in disk fractions in several regions as an exponential decay with a typical time scale of $2.5\,\mathrm{Myr}$. Similar estimates have been found from several other star forming regions and star clusters (e.g. Lada et al., 2006; Sicilia-Aguilar et al., 2006; Winston et al., 2007; Hernández et al., 2007; Gutermuth et al., 2008; Sung et al., 2009; Ansdell et al., 2016, 2017).

Disc dispersal is the result of the interplay of many different processes. While there are several environmental effects which can accelerate it (see Section 3), within this section we limit our discussion only to internal causes.

The first mechanism leading to mass loss is the viscous evolution of the disks. The distribution of angular momentum causes both the expansion of the disk and accretion onto the host star (Armitage, 2011; Williams & Cieza, 2011). Measurements of stellar accretion rates show that Class II objects are constantly accreting mass into the star from the disks. A $\sim 1\,\mathrm{M_\odot}$ young star can accrete up to 10% of its mass during the first Myr of the Class II phase, with accretion rates $10^{-8} - 10^{-7}\,\mathrm{M_\odot\,yr^{-1}}$ (Hartmann et al., 1998, 2016). These accretion rates decrease with stellar age (e.g. Sicilia-Aguilar et al., 2010; Manara et al., 2012, 2016) and decline even further in transition disks, which are on the verge of completely being depleted of gas (Kim et al., 2016; Najita et al., 2015). This decline with age is expected from accretion theory (Hartmann et al., 1998). However, disk dispersal through accretion only would imply an indefinite viscous expansion of the outer regions of the disks. Since there is no observational evidence for this, there must be other processes aiding in mass dissipation (Gorti et al., 2009).

Another elemental process that causes mass depletion in disks is planet formation. Observational and theoretical studies have shown that planet formation must start within 0.1 to 1 Myr after star formation for disks to still be massive enough to form rocky planets and the cores of gas giants (e.g. Greaves & Rice, 2010; Williams, 2012; Najita & Kenyon, 2014; Manara et al., 2018; Tychoniec et al., 2020, Chapters 3, 4, and 5 of this thesis). Resolved observations of circumstellar disks have shown gaps and spiral arms that are likely produced by young planets (e.g. Isella et al., 2012; Andrews et al., 2016; van Boekel et al., 2017; Marino et al., 2018, 2019; van der Marel et al., 2018; Francis & van der Marel, 2020; Huang et al., 2020). Numerical models have confirmed that these structures can be originated by planet formation (e.g. Bae et al., 2018;
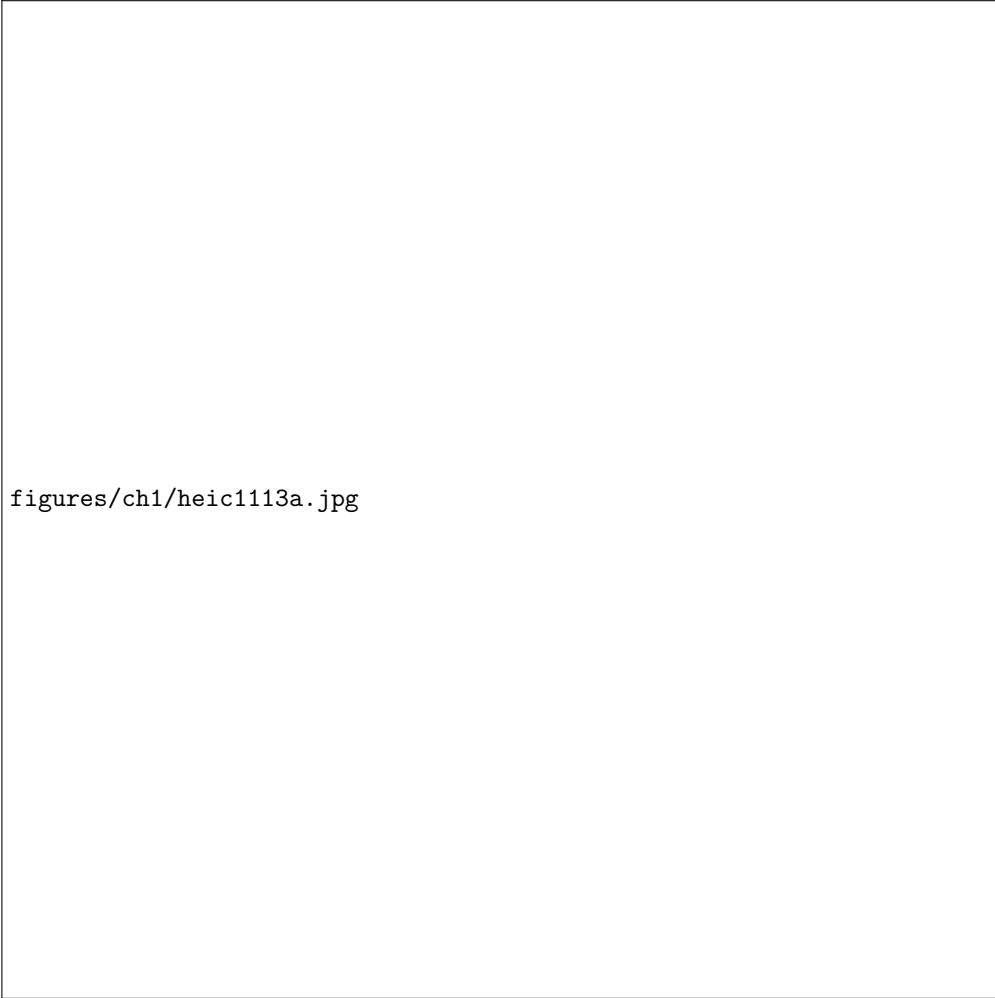
figures/ch1/heic1113a.jpg

Figure 3: Protostellar jets and outflows in HH47 (top panel, Vela constellation), HH34 and HH2 (bottom panels, Orion nebula). *NASA, ESA, and P. Hartigan (Rice University).*

Dong et al., 2018).

An internal mechanism that can accelerate disk dispersal is photoevaporation from the host star. Internal photoevaporation is the process through which high-energy photons coming from the host star heat the disk surface, causing gas to evaporate (e.g. Luhman et al., 2010; Ercolano et al., 2011; Gorti et al., 2009). Internal photoevaporation is dominated by X-ray photons (Owen et al., 2012). The bulk of the internal photoevaporation mass loss occurs in the inner 20 au of the disks (Font et al., 2004; Owen et al., 2010). This process can then also constrain the time available to form planetary systems (Gorti et al., 2015). However, photoevaporation seems to be more efficient when the radiation comes from nearby stars. We expand on this process on Section 3.

2.2 Disc masses and sizes

Circumstellar disks are formed by gas and dust and, unlike in the interstellar medium, these two components are decoupled. Most of the mass in solids is in the shape of dust grains of sizes $\sim 1\,\mathrm{mm}$ and larger, which are not mixed with the gas (Bergin & Williams, 2018). To determine disk masses and sizes, both of these constituents need to be addressed separately.

The gas is generally much harder to detect than the dust. This is because its main constituent, molecular hydrogen, is affected by several physical processes which make it very weak or even undetectable in most of the disk (Field et al., 1966; Carmona et al., 2008). Other molecules can be used as tracers of molecular hydrogen, such as carbon monoxide and hydrogen deuteride. However, the abundance of these molecules has to be determined with very high precision to be used as a tracer for molecular hydrogen (Bergin & Williams, 2018). As such, total disk masses are generally estimated from disk dust masses.

Dust masses are measured by proxy. The millimetre wavelength flux measure can be transformed into a disk dust mass using the relation:

$$\mathrm{M_{dust}} = \frac{F_\nu d^2}{\kappa^2 B_\nu(T_{\mathrm{dust}})} \tag{13}$$

where F_ν is the millimetre flux, κ is the estimated opacity, B_ν is the Plank function and T_{dust} is the temperature of the disk midplane, assumed constant and $\approx 20\,\mathrm{K}$ (Andrews & Williams, 2005). From the dust mass, a gas mass is calculated by assuming a 100:1 gas-to-dust ratio. This ratio is derived from the interstellar medium (Goldsmith et al., 1997).

There is a big range of observed disk masses, and they seem to greatly depend on the age (see Section 2.1) and environment (see Section 3) of the disks. In surveys of the youngest star forming regions, such as Chamaeleon I and the Lupus clouds, total disk masses span a range from $\sim 10^{-1}$ to $10\,\mathrm{M_{Jup}}$ (Ansdell et al., 2016; Pascucci et al., 2016; Ansdell et al., 2017). In older regions, such as Upper Scorpio, the average disk mass is $\sim 1\,\mathrm{M_{Jup}}$ (Barenfeld et al., 2016).

Measuring disk sizes requires the disks to be resolved, making it more complicated than disk masses. Surveys at high angular resolution, such as those carried out by ALMA, allow for measurements of disk dust sizes. However, radial drift of dust means that the measured dust sizes are likely to be more compact than the gas disks. Gas disk sizes are measured through the rotational line emission from molecules such as carbon monoxide and cyanogen (e.g. Barenfeld et al., 2017; Facchini et al., 2017; Ansdell et al., 2018; Trapman et al., 2019). Ansdell et al. (2018) find the ratio of gas radius to dust radius to be $\sim 1.5-3$. Dust disk sizes in the Lupus clouds have been found to range from $\sim 40\,\mathrm{au}$ to $\sim 300\,\mathrm{au}$ (Ansdell et al., 2018). In Upper Scorpio, the median disk dust radius is 21 au (Barenfeld et al., 2017).

3 Effects of the environment on circumstellar disk evolution

Demographic studies of circumstellar disks show great variations between regions of different ages and stellar densities. In regions where massive stars are present, the number of disks and their masses decrease the closer they are to an OB-type star. Several studies have found diminishing disk fractions, disk masses, and disk sizes with decreasing distance to θ^1 Ori C, an O6 type star in the Trapezium cluster (e.g. Vicente & Alves, 2005; Mann & Williams, 2010; Mann et al., 2014; Eisner et al., 2018). In particular, there is a lack

of disks with dust masses higher than $9\mathrm{M}_\oplus$ within $0.03\,\mathrm{pc}$ of θ^1 Ori C. At projected distances larger than $0.3\,\mathrm{pc}$ from the star, the disk population is more similar to those of low mass star forming regions (Vicente & Alves, 2005; Mann et al., 2014). Similar effects are reported by Ansdell et al. (2017) in the σ Orionis region, where disk masses lessen with decreasing distance to the OB triple star system at its center. No massive disks are detected within the $0.5\,\mathrm{pc}$ around these massive stars. van Terwisga et al. (2020) find evidence for two distinct disk populations in the NGC 2024 region: one population, located close the massive star IRS 1, appears to have fewer disks and lower disk masses than the second population, embedded in a dense molecular gas ridge. Several other surveys have revealed evidence of environmental effects in various regions, such as NGC 6611 (Guarcello et al., 2009), Pismis 24 (Fang et al., 2012), NGC 1977 (Kim et al., 2016), and Cygnus OB2 (Guarcello et al., 2016).

Disc mass distributions in low mass star forming regions are found to be statistically indistinguishable from each other. This is the case for Lupus, Taurus, and the Orion Molecular Cloud 2 (Ansdell et al., 2016; van Terwisga et al., 2020), suggesting that in low stellar densities the disks evolve similarly and mostly unperturbed. These regions, together which others such as Chamaeleon I and Ophiuchus (Williams et al., 2019), represent relatively young and sparse locations of star formation, with estimated ages of $1-5\,\mathrm{Myr}$. The disks masses in all of these regions are in average higher than those in Orion, even though their ages are comparable. Older regions, such as Upper Scorpio ($\sim 10\,\mathrm{Myr}$, Barenfeld et al., 2016), have less disks than younger ones and the disks are less massive and smaller (Barenfeld et al., 2016, 2017).

While it is known that disk mass decreases with age due to viscous evolution (see Section 2.1), these observations suggest that the stellar density of the star forming region and the presence of massive stars in the vicinity can also affect disk mass distributions. These differences in disk populations can be attributed to a series of environmental effects which are described below.

3.1   Dynamical truncations

While star-star collisions are rare, the cross sections of circumstellar disks are much larger than those of stars, so their probability of being perturbed dynamically by another star in a crowded environment is non negligible (Pfalzner, 2003). Given that the encounters themselves are very short-lived, the observational evidence of dynamical encounters is limited to the imprints they can leave on the disks. Population studies of disks in dense stellar regions, in particular those in which the size of the disks can be resolved, have shown that the average disk size decreases with increasing local stellar density (e.g. Vicente & Alves, 2005; de Juan Ovelar et al., 2012). This was proposed as a result of dynamical encounters truncating the disks.

With the advent of modern telescopes such as ALMA and the VLT it has been possible to observe the eventual consequences of dynamical encounters directly. A fascinating assortment of disk substructure is now coming to light, such as spiral arms, tidal tails, and misaligned inner and outer disks. These could be explained by close encounters with passing stars (e.g. Reche et al., 2009; Christiaens et al., 2014; Salyk et al., 2014; Kuffmeier et al., 2019; Kraus et al., 2020; Menard et al., 2020). Cabrit et al. (2006) suggest that the $\sim 600\,\mathrm{au}$ trailing "tail" of material observed in the disk of RW Aur A was likely caused by the recent fly-by of its companion, RW Aur B. Numerical simulations by Dai et al. (2015) confirm that this might indeed have been the case, since the arms seen in RW Aur A look like the ones that form when a star passes nearby the disk in their simulations. New observations by Rodriguez et al. (2018) reveal more substructure within the disk of RW Aur A, and the authors argue that this might be the result of several, cumulative close encounters. Winter et al. (2018c) model the dust emission structure surrounding the triple system HV Tau and the disk of DO Tau, and suggest that it corresponds to the remainders of the disks surrounding both system after they experienced a close encounter about $0.1\,\mathrm{Myr}$ ago.

Furthermore, it has been proposed that the young protoplanetary disk of the solar system was truncated in such an encounter. This argument is based on the sharp edge of the solar system at $\sim 30\,\mathrm{au}$, which can be attributed to an encounter with a star of around a solar mass at a periastron distance of $\sim 100\,\mathrm{au}$ (Adams, 2010; Breslau et al., 2014; Pfalzner et al., 2018). Additional evidence for this encounter is given by the orbits of the *Sednitos*, a family of a dozen (known) solar system objects including the dwarf planet Sedna, which have extraordinary wide orbits ($a > 150\,\mathrm{au}$) and a perihelion distance much larger than the Earth's. Jílková et al. (2015) show that the orbits of the *Sednitos* can be explained by their origin being a capture from the planetesimal disk of a nearby passing star. Pfalzner et al. (2018) show that a fly-by of a star with mass 0.3 to $1\,\mathrm{M}_\odot$ at perihelion distances between 50 and $150\,\mathrm{au}$ could cause such characteristics, and that the *Sednitos*

could have originally belonged to the solar system and their orbits have been excited by such an encounter.

The first numerical studies regarding the effects that a nearby star could have on a circumstellar disk were performed in the context of binary star formation and evolution (e.g. Paczynski, 1977; Pringle, 1989; Clarke & Pringle, 1991). It was a natural step to expand these analyses into the realm of larger stellar systems, where the perturber is a point mass in an unbound orbit. Clarke & Pringle (1993) perform numerical simulations of prograde, retrograde coplanar and orthogonal approaches of a star to a circumstellar disk. They investigated the fate of the debris resulting from these encounters: how much remains bound, how much is unbound, and how much stays in the neighbourhood of the disk. They find that a prograde coplanar encounter is the most destructive, that disk matter down to about $0.5r_{enc}$ is left unbound after the encounter, and that a considerable amount of matter is captured by the perturbing star.

Several numerical simulations have continued to explore the effects of dynamical encounters over circumstellar disks (e.g. Korycansky & Papaloizou, 1995; Hall et al., 1996; Bonnell & Kroupa, 1998; Pfalzner, 2003; Bate et al., 2003; Pfalzner et al., 2005b,a; Breslau et al., 2014; Vincke et al., 2015; Vincke & Pfalzner, 2016). Scally & Clarke (2001) simulate a region akin to the Trapezium cluster and keep track of all the encounters occurring in 12 Myr. They find that it is likely for each star in their model to experience at least one encounter closer than 1×10^3 au during the 1×10^6 Myr estimated disk lifetimes. However, they determine that only 3% to 4% of the disks can be destroyed by encounters alone. They consider an encounter to be destroying if the perturber comes closer than 100 au. Further analyses have shown that, unlike the assumptions by Scally & Clarke (2001), it is not only one very close encounter that can destroy a disk, but actually a series of further encounters can have a cumulative effect (Pfalzner et al., 2006). Further models have shown that dynamical encounters might not only truncate the disks but also harden their surface density (Rosotti et al., 2014), lead to the formation of spiral arms, and cause accretion bursts into the stars due to material being pushed inwards on the disk. Pfalzner et al. (2005a) show that these bursts of accretion are common in regions such as the Orion Nebula Cluster.

In recent years, newer simulations suggest that while dynamical encounters do play a role in shaping circumstellar disks, they are not the most efficient or most important method for disk destruction in high stellar density environments. Winter et al. (2018b) perform a comparison of disk mass loss rates caused by external photevaporation and dynamical truncations. They find that, while some disks do get truncated in close encounters, the mass loss due to external photoevaporation is orders of magnitude higher. Winter et al. (2018a) find that even the cumulative effect of many distant dynamical encounters does not lead to a great amount of mass loss. As will be discussed in Section 3.2 and Chapters 3, 4, and 5 of this thesis, the relative importance of dynamical encounters as a means for efficient disk destruction is still up for debate, in particular when compared to external photoevaporation.

3.2   External photoevaporation

Photoevaporation is the process by which high energy photons heat the surface of a circumstellar disk and evaporate material from it. These photons can originate from the host star or from nearby massive stars in the vicinity of a disk. The former process is known as internal photoevaporation (see Section 2.1), and the latter as external photoevaporation. Given that external photoevaporation is the one directly related to the star formation environment, in this section and throughout this thesis the main focus is on that mechanism.

There are several observational clues of external photoevaporation removing mass in circumstellar disks. The first observations correspond to *proplyds*, cometary tail-like structures of ionized gas that form in disks when close to a massive star. The first proplyds were observed in the Orion nebula (O'dell & Wen, 1994; O'dell, 1998; Vicente & Alves, 2005; Eisner & Carpenter, 2006; Mann et al., 2014; Kim et al., 2016) and several subsequent studies confirmed that their structures could be explained by the massive stars in the region stripping mass from the disks through radiation (e.g. Richling & Yorke, 1997; Johnstone et al., 1998; Störzer & Hollenbach, 1999; Adams et al., 2004). The demographic differences across star forming regions enumerated at the beginning of this section also show that discs closer to bright stars are less massive than disks located in sparser regions. While in high density regions dynamical encounters might contribute to disk dispersal, observations seem to point to proximity to an OB star resulting in declining disk masses.

Photoevaporation can occur from a combination of far ultraviolet (FUV), extreme ultraviolet (EUV), and X-ray photons. EUV radiation ionizes and heats disk surfaces up to $\sim 10^4$ K, while FUV and X-ray heat gas up to temperatures from ~ 100 to 3000 K but keep it neutral. FUV photons dissociate gas molecules,
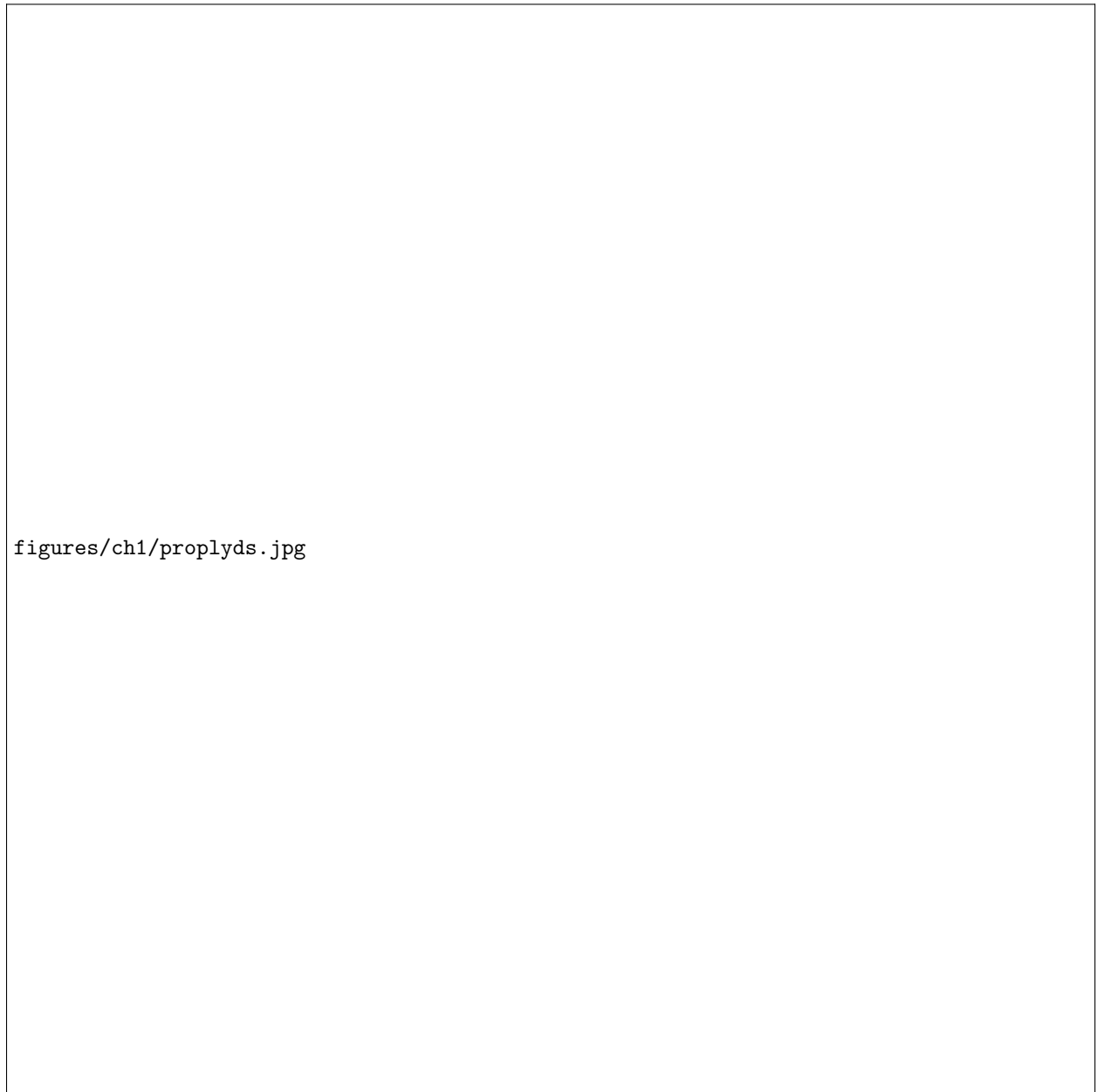
Figure 4: Proplyds in the Orion nebula observed with the Hubble Space Telescope. *NASA/ESA, L. Ricci (ESO)*.

generating a photodissociation region of neutral gas which the EUV radiation can not penetrate. Because of this, FUV radiation is the main driver of external photoevaporation (Johnstone et al., 1998; Adams et al., 2004).

The thermal pressure from the photons pushes the gas outward. The bulk of the mass loss occurs from the outer regions of the disks, beyond a critical radius r_g at which the sound speed of the heated gas equals the escape speed from the gravitational field of the host star. This radius is defined as:

$$r_g = \frac{GM_* <\mu>}{kT} \approx 100 \, \text{au} \left(\frac{T}{1000\text{K}}\right)^{-1} \left(\frac{M_*}{M_\odot}\right) \tag{14}$$

where M_* is the mass of the host star and $<\mu>$ is the average mass of the gas particles (Adams et al., 2004). Early theoretical models of photoevaporation assumed that mass loss due to photoevaporation occurred only at radii $r > r_g$ (e.g. Hollenbach et al., 1994; Johnstone et al., 1998; Störzer & Hollenbach, 1999), and that as such it would result only in disk truncation. Adams et al. (2004) show that mass is still removed from the inner regions of the disks, but the effects of external photoevaporation do cause the disks to deplete from the outside in. While the thermal pressure affects the behaviour of the gas, dust grains with radii $\leq 1 \, \text{cm}$ (Adams et al., 2004) can get entrapped in the photoevaporation wind and also be removed from the disks. However, dust quickly agglomerates to sizes larger than the critical radius and turns resilient to photoevaporation (Haworth et al., 2018).

Studies of single disks as well as clustered regions show disk masses to be strongly dependent on the background radiation fields, as a direct consequence of external photoevaporation. The intensity of the radiation fields is generally defined in terms of Habing units (G_0), with $1 \, G_0 \approx 1.6 \times 10^{-3} \, \text{erg cm}^{-2} \, \text{s}^{-1}$ being the average flux in the local interstellar medium (Habing, 1968). Adams et al. (2004) find that disks around stars $M_* \approx 0.5 \, M_\odot$ are evaporated down to $\sim 15 \, \text{au}$ in less than 10 Myr when exposed to moderate radiation fields of $\sim 3000 \, G_0$, but that even disks around stars of a solar mass or higher are destroyed in that time scale for radiation fields $\sim 3 \times 10^4 \, G_0$. Anderson et al. (2013) find that disk dispersal is nearly always dominated by external photoevaporation in FUV fields $\sim 3000 \, G_0$. Newer models have shown that even lower radiation fields can be destructive to circumstellar disks. Facchini et al. (2016) show that disks of size $\sim 150 \, \text{au}$ are subject to strong mass loss due to photoevaporation in radiation fields as low as $\sim 30 \, G_0$. This dependence on background radiation fields can be directly linked to a dependence on local stellar density.

Several numerical models have been developed to analyse the effects of external photoevaporation in clustered environments. Scally & Clarke (2001) model a region similar to the centre of the ONC and find external photoevaporation to cause important mass loss on disk radii larger than 10 au. According to their mass loss rates, for planets to be able to form beyond that radii, they should already be assembled within 2 Myr of the formation of the disk. They also find external photoevaporation to be dominant over dynamical truncations as a means for disk destruction. Similar results are obtained by Adams et al. (2006) and Fatuzzo & Adams (2008), who statistically estimate the FUV background radiation fields in simulated star clusters, and find values enough to truncate disks down to $\sim 30 \, \text{au}$ within 10 Myr. Fatuzzo & Adams (2008) argue that 25% of the disk population loses planet-forming potential in a star cluster similar to those found in the solar neighbourhood ($N_* = 1000 - 2000$).

Newer models have confirmed the relative importance of external photoevaporation as a method for disk dispersal, in particular in clustered environments. Winter et al. (2018b) find that in regions where the local stellar density is enough for dynamical truncations to be possible ($N_* \gtrsim 10^4 \, \text{pc}^{-3}$), the disks are also exposed to FUV fields $\sim 3000 \, G_0$ which causes the destruction of even the most massive disks ($M_{\text{disk}} = 0.1 M_\odot$) within 3 Myr. They conclude that it is highly unlikely to have clustered environments where dynamical truncations dominate over external photoevaporation. In follow up work, Winter et al. (2020) perform simulations of regions of different densities and compare the effects of external photoevaporation and dynamical truncations. They find photoevaporation to be the dominant mass loss process in regions similar to the Central Molecular Zone of the Milky Way (surface density $\Sigma_0 = 10^3 \, M_\odot \, \text{pc}^{-2}$) as well as in densities closer to the solar neighbourhood ($\Sigma_0 = 12 \, M_\odot \, \text{pc}^{-2}$). In the dense regions, external photoevaporation evaporates 90% of circumstellar discs within 1.0 Myr. Similar results are reported by Nicholson et al. (2019), who find 50% of disks are evaporated due to external photoevaporation within 1.0 Myr in regions of density $\sim 100 \, M_\odot \, \text{pc}^{-3}$. Chapters 3, 4, and 5 of this thesis obtain similar disk dispersion timescales for external photoevaporation, and confirm that this process seems to be dominant over dynamical truncations even in high density regions.

As proximity to massive stars is the defining factor of external photoevaporation, the extent of the effects of radiation depend greatly on the spatial distribution of the star forming regions. In particular, the presence of gas can shield the circumstellar disks from radiation, allowing them to live for longer. van Terwisga et al. (2020) report the discovery of two distinct disk populations in the NGC 2024 region. One is a population of low mass disks, similar to the ones observed in regions with higher stellar densities such as the ONC. They are affected by the radiation of the massive stars IRS 1 and IRS 2b, and their low masses can be explained by external photoevaporation. The second population of disks is embedded in a dense ridge of molecular gas, and the disk masses are higher and similar to those of low density regions such as Lupus or Taurus. The authors argue that is possible for these disks to be more massive because the gas protects them from external photoevaporation. Winter et al. (2019) reproduce the observed disk population in the Cygnus OB2 region by considering the presence of gas in the early stages of the cluster. The gas absorbs some of the radiation coming from massive stars, shielding the disks from photoevaporation during their first million years of evolution.

Numerical and observational evidence points to external photoevaporation being the most important environmental mechanism affecting the evolution of circumstellar disks. Its effects are one of the main foci of this thesis and are explored in Chapters 3, 4, and 5.

3.3   Ram pressure stripping

The star formation process results not only in stars and circumstellar disks, but also in leftover gas, which can linger for several million years before eventually being expelled due to stellar feedback (Portegies Zwart et al., 2010). This gas can have important effects on the stellar dynamics of the region (see Section 1) and on the evolution of the circumstellar disks. As was discussed in Section 3.2, gas can shield the disks from external photoevaporation, reducing their mass loss rates and extending their lifetimes. However, the presence of gas can also truncate the disks via ram pressure stripping.

Ram pressure stripping was first investigated in the context of galaxies moving through the intra (galaxy) cluster medium. Depending on the gravitational force, the drag from the gas can remove material from the outer parts of the disks. Theoretical truncation radii have been calculated for galaxies (Gunn & Gott, 1972; Mori & Burkert, 2000) and later expanded to disks moving through the interstellar medium (Chevalier, 2000; Moeckel & Throop, 2009; Wijnen et al., 2017a). After ram pressure has stripped the outer regions, the subsequent disk evolution is dominated by a redistribution of angular momentum. This is caused by the accretion of material with zero azimuthal angular momentum from the interstellar medium onto the disk, which decreases the local momentum on its surface. This process increases the surface density of the disks and shrinks them further. However, this shrinking is much less pronounced than during the stripping phase (Wijnen et al., 2017a).

Wijnen et al. (2016) find ram pressure stripping shrinks initially $100\,\mathrm{au}$ disks down to $\sim 20\,\mathrm{au}$ within $2500\,\mathrm{yr}$ of evolution. Furthermore, Wijnen et al. (2017b) find ram pressure stripping to be the dominant disk truncation mechanism when compared to dynamical encounters, in embedded clusters where 30% of the mass is in stars, regardless of the total mass of the cluster. The inner regions of the disk are not affected by the ram pressure. However, Moeckel & Throop (2009) find more modest mass loss rates in disks affected by ram pressure stripping, and they estimate than this process might lead to mass losses of no more than $\sim 2\%$ the initial mass of the disks.

3.4   Supernovae

A nearby supernova explosion can affect a circumstellar disk in two main ways: the blast of the explosion can remove mass from the disk through ram pressure stripping (Chevalier, 2000) and it can also enrich the young disk with short-lived radionuclides (SLRs), such as ^{26}Al and ^{60}Fe. The excess of SLRs in meteorites with respect to the average interstellar medium suggests that these isotopes were not inherited at the moment of the formation of the solar system disk, but where actually injected through a later event (e.g. Russell et al., 2006; Gounelle & Meibom, 2008).

Close & Pittard (2017) perform simulations of a supernova explosion located at $0.3\,\mathrm{pc}$ of a circumstellar disk. They find that low mass disks ($\mathrm{M}_d \sim 0.1\ \mathrm{M}_{Jup}$) can only survive such an event if they face the blast of the supernova edge-on, but even in that case they lose $\sim 60\%$ of their initial mass. In simulations where

disks are inclined with respect to the blast direction, they can lose up to 90% of their mass within 100 years. Higher mass disks ($M_d \sim 1.0~M_{Jup}$) can lose up to 30% of their mass in the blast. This mass loss occurs through ram pressure stripping during the first 100 years, in what the authors deem a period of instantaneous stripping. This quick mass loss is followed by a longer, moderate ablation period which lasts until $\sim 200\,\mathrm{yr}$ after the explosion. While the intensity of the ablation decreases in time, through this period the mass loss rates are still 2 orders of magnitude higher than those of external photoevaporation.

Portegies Zwart et al. (2018) study the effects that a nearby supernova explosion can have on a circumstellar disk around a solar mass star and initial radius 100 au. They find that the disk is almost completely stripped of its mass if the supernova occurs at a distance of 0.05 pc. At distances from 0.15 to 0.4 pc the disks are truncated down to $\sim 50\,\mathrm{au}$. There is mass loss between 10 and 50 au, but the inner 10 au region remains unperturbed. However, they find that in their models the SLRs enrichment is too low to explain the excess observed in the solar system meteorites.

Ansdell et al. (2020) present a survey of disks in the λ Orionis region, in which there is evidence of a supernova explosion $\sim 1\,\mathrm{Myr}$ ago. They find that, while no disks are observed within 0.3 pc from the estimated location of the explosion, the rest of the disks seem to follow the expected mass distributions from simple age evolution processes, given that this is an older region (age $\sim 5\,\mathrm{Myr}$). They suggest that a supernova occurring several million years into disk evolution might not be destructive enough to remove planet forming potential from the disks, except for the ones located extremely close to the explosion.

4   Numerical simulations

The nature of astrophysical phenomena makes it practically impossible to analyse our subjects of study directly. The invention of the telescope revolutionized astronomy, and the modern telescopes of today have opened our eyes to a wonderful array of observations that Lippershey and Galilei could not have dreamed of. And yet, all we can observe are nothing but instantaneous snapshots of extremely complicated and convoluted processes which, save for particular exceptions, evolve in timescales of millions of years.

While pure theory can give us a mathematical understanding of astrophysical phenomena, there is a different comprehension that comes from seeing the processes evolve before our eyes. It is in this sense that numerical simulations provide an invaluable asset to astrophysicists: by bridging the gap between observations and theory. Processes that in nature take several million years can be simulated in weeks in a computer. While many assumptions have to be made to be able to create computational simulations, the insight that numerical models provide make them an essential piece of modern astrophysics.

This thesis deals with astrophysical simulations of processes that occur at many different time and spatial scales. To be able to model the complex systems that compose this work, we make use of the Astrophysical MUltipurpose Software Environment (AMUSE), which allows to bring together numerical codes for many different astrophysical processes. In the following sections we explain some general numerical methods relevant to this thesis and introduce the AMUSE framework.

4.1   N-body codes

Gravitational interactions between particles are described by Newton's equations of motion. These equations allow us to determine the position and velocity of a particle at any given time:

$$\ddot{\mathbf{r}}_i = -G \sum_{j=1, j \neq i}^{N} m_j \frac{\mathbf{r}_i - \mathbf{r}_j}{|\mathbf{r}_i - \mathbf{r}_j|^3} \tag{15}$$

where $\mathbf{r}_i$ is the position of particle i with respect to an inertial frame, m_i is its mass, and G is the universal gravitational constant (Newton, 1687). Analytical solutions for this system of equations are known only for $N = 2$ and particular cases of $N = 3$ (the restricted three-body problem). However, for any instances of $N > 3$, the equations of motion must be solved numerically.

N-body codes refer to a category of numerical solvers in which each astrophysical object (or sometimes a group of objects) is deemed as one single particle, and the equations of motion are solved numerically for each of the N particles. In astrophysics, N-body integrators are generally used to model planetary systems (e.g. Spurzem et al., 2009; Cai et al., 2017; van Elteren et al., 2019; Torres et al., 2019), stellar dynamics

(e.g. Casertano & Hut, 1985; Scally & Clarke, 2001; Fujii & Portegies Zwart, 2016; Portegies Zwart, 2016), and galaxy formation and dynamics (e.g. Springel et al., 2005; Boylan-Kolchin et al., 2009; Klypin et al., 2011; Baugh et al., 2019).

At the core of an N-body solver is the time discretization used to iterate over Eq. 15. The most used method to solve the system of equations is known as the predictor-corrector scheme. This is an implicit method, meaning that the equation to calculate the state of the system at time $t + \delta t$ actually contains the expression $t + \delta t$. These implicit equations are solved iteratively. First, the predictor step uses Taylor series to expand $t + \delta t$ and extrapolate positions and velocities at time t. The accelerations and higher derivatives are then recalculated with the extrapolated values, and a combination of old and new accelerations are used to predict higher derivatives. Finally, the corrector step uses these new derivatives to refine the predictions by adding terms to the Taylor expansion. The highest exponent in the Taylor expansion is usually referred to as the order of the integrator.

Different types of N-body codes exist. Pure N-body codes allow for no free parameters other that the time step for the iterations. These codes generally scale with N as $\mathcal{O}(N \log N)$. Direct N-body codes make use of additional parameters to speed-up the calculations and usually make use of regularizations to resolve close multiple systems, making them appropriate for very dense, collisional simulations. However, these types of codes scale as $\mathcal{O}(N^2)$. Approximate N-body codes relax constraints on the calculations, such as precision, to achieve very fast results. These codes are usually based on tree calculations and particles meshes, and they usually scale as $\mathcal{O}(N \log N)$ with some of them even reaching $\mathcal{O}(N)$.

4.2 Smoothed-particle hydrodynamics

While N-body codes are useful for modelling many astrophysical systems, it is clear that they scale with the number of physical particles. If what we want to model is a fluid or gas, such as a molecular cloud, N-body codes are not the most appropriate. Modelling each gas particle as a particle in an N-body code is not computationally feasible. For such cases, smoothed-particle hydrodynamics (SPH) codes are a better alternative.

There are two types of SPH codes. Lagrangian codes are based on particles, but the definition of an SPH particle is different than that of an N-body code. An SPH particle is a discrete element of fluid, but it does not directly represent a physical particle. The properties of an SPH particle, such as its position and velocity, are calculated as the weighted average of the surrounding particles. Each SPH particle is defined by a smoothing length, which determines the weight given to the surrounding particles. This weight decreases steeply around each particle, greatly reducing the number of calculations between elements. The second type of SPH codes correspond to Eulerian methods, where the hydrodynamics differential equations are solved in a grid.

Hydrodynamics codes are used to model several phenomena in astrophysics, such as supernovae explosions, stellar mergers, star formation and stellar feedback (e.g. Bate, 1998; Klessen et al., 1998; Bate et al., 2003; Bate, 2012; Pelupessy & Portegies Zwart, 2012; Fujii & Portegies Zwart, 2015; Dobbs et al., 2020), and galaxy formation and large scale cosmological structure (e.g. Hernquist et al., 1996; Springel & Hernquist, 2003; Schaye et al., 2015; Mitchell et al., 2017).

4.3 AMUSE

The Astrophysical MUltipurpose Software Environment (AMUSE[2]) is a `python` framework which allows for integration of several independent numerical codes, facilitating their combination and allowing to model more complex physical systems (Portegies Zwart et al., 2009, 2013; Pelupessy et al., 2013; Portegies Zwart & McMillan, 2018). The AMUSE project is motivated and built on three core principles (Portegies Zwart & McMillan, 2018):

1. Provide an homogeneous and physically motivated interface for existing codes for astrophysical simulations

2. Integrate multiple community codes from four fundamental physical domains: stellar evolution, gravitational dynamics, hydrodynamics, and radiative transfer

---

[2]http://amusecode.org

17

3. Allow to design new simulation experiments by combining the community codes in different ways

Currently, AMUSE incorporates more than 60 community codes. The open source and community oriented philosophy of the project allows for anybody to contribute by creating an AMUSE interface to integrate new astrophysical simulation codes. In the context of this thesis, AMUSE was used to couple codes for stellar dynamics and stellar evolution together with an implementation for viscous disk evolution and photoevaporation. The AMUSE interface used to integrate the viscous evolution code, VADER (Krumholz & Forbes, 2015, see Chapter 3 for more information), was developed for the simulations performed in Chapters 3, 4, and 5 of this thesis.

5   This thesis

The goal of this thesis is to quantify the effects that the star formation environment has over the evolution of young circumstellar disks. In particular, the focus is on external photoevaporation and dynamical truncations, and on how these two mechanisms compare in terms of mass loss rates. We evaluate the significance of each effect by analysing the resulting distributions of disk masses, and we perform comparisons with disk masses observed in star forming regions.

This work has been developed through numerical simulations of star forming regions. Our models consider stellar dynamics, stellar evolution, viscous disk evolution, external and internal photoevaporation, and dust evolution in the discs. All the astrophysical codes necessary to assemble the simulations developed for this thesis were bridged together using the AMUSE framework (Section 4.3).

In **Chapter 2** we simulate young star clusters which are embedded in gas. We use a background potential to implement the gravitational effects of the gas, and a semi-analytical model for the viscous evolution of the discs. We then evolve the stellar dynamics of the region for 2 Myr, during which the discs are susceptible to truncation due to close encounters with other stars. We study the resulting distributions of disc sizes under three scenarios: clusters with no gas, with constant gas throughout the entire simulation, and with gas expulsion starting at 1 Myr. We also perform a basic comparison to disc distributions observed in several star forming regions.

In **Chapter 3** we compare the effects of dynamical truncations against external photoevaporation, in terms of mass loss. We introduce a new model for the discs, which uses a viscous evolution code. For modelling external photoevaporation we use a pre-computed grid of mass loss rates, which allows us to determine the mass loss in every time step depending on the radius of the disc and its distance to a massive star. We model stars clusters of densities 50 $M_\odot$ pc^{-3} and 100 $M_\odot$ pc^{-3} and evolve the stellar dynamics (including dynamical encounters), stellar evolution, viscous evolution of the discs, and external photoevaporation.

In **Chapter 4** we use the model from Chapter 3 to quantify the local stellar densities for which external photoevaporation severely constrains disc lifetimes. We investigate a larger parameter space of number stellar densities than in Chapter 3 and look at the disc mass distributions after 2 Myr of evolution. We compare our results to observations of disc masses in different star forming regions.

In **Chapter 5** we improve on the initial conditions of previous models by simulating not only the disc evolution, but also the star formation process. We implement a simple model of giant molecular cloud collapse and star formation to obtain primordial positions, velocities, and masses of the stars. We then use these as initial conditions for our stellar dynamics and disc evolution model. In this Chapter we also expand our circumstellar disc model by adding the effects on internal photoevaporation and dust evolution inside the disc.

The results of this thesis show that mass loss due to external photoevaporation dominates over dynamical encounters in all the simulated stellar regions. External photoevaporation is extremely efficient in evaporating circumstellar discs, completely depleting the mass of $\sim 50\%$ of the initial discs in low density regions (Chapter 3) and up to 90% of the discs in high density regions (Chapter 4) after 2 Myr of evolution.

References

Adams F. C., 2010, , 48, 47

Adams F. C., Myers P. C., 2001, , 553, 744

Adams F. C., Hollenbach D., Laughlin G., Gorti U., 2004, , 611, 360

Adams F. C., Proszkow E. M., Fatuzzo M., Myers P. C., 2006, , 641, 504

Anderson K. R., Adams F. C., Calvet N., 2013, , 774, 9

Andrews S. M., Williams J. P., 2005, The Astrophysical Journal, 631, 1134

Andrews S. M., Wilner D. J., Hughes A. M., Qi C., Dullemond C. P., 2010, , 723, 1241

Andrews S. M., et al., 2016, The Astrophysical Journal Letters, 820, L40

Ansdell M., et al., 2016, , 828, 46

Ansdell M., Williams J. P., Manara C. F., Miotello A., Facchini S., van der Marel N., Testi L., van Dishoeck E. F., 2017, , 153, 240

Ansdell M., et al., 2018, , 859, 21

Ansdell M., et al., 2020, arXiv:2010.00012 [astro-ph]

Appenzeller I., Tscharnuter W., 1975, Astronomy and Astrophysics, 40, 397

Armitage P. J., 2011, , 49, 195

Bae J., Pinilla P., Birnstiel T., 2018, , 864, L26

Bally J., 2016, Annual Review of Astronomy and Astrophysics, 54, 491

Barenfeld S. A., Carpenter J. M., Ricci L., Isella A., 2016, , 827, 142

Barenfeld S. A., Carpenter J. M., Sargent A. I., Isella A., Ricci L., 2017, , 851, 85

Bate M. R., 1998, The Astrophysical Journal Letters, 508, L95

Bate M. R., 2010, , 404, L79

Bate M. R., 2011, , 417, 2036

Bate M. R., 2012, Monthly Notices of the Royal Astronomical Society, 419, 3115

Bate M. R., Bonnell I. A., Bromm V., 2003, Monthly Notices of the Royal Astronomical Society, 339, 577

Baugh C. M., et al., 2019, Monthly Notices of the Royal Astronomical Society, 483, 4922

Baumgardt H., Kroupa P., 2007, Monthly Notices of the Royal Astronomical Society, 380, 1589

Baumgardt H., Makino J., 2003, Monthly Notices of the Royal Astronomical Society, 340, 227

Bergin E. A., Williams J. P., 2018, arXiv e-prints, p. arXiv:1807.09631

Bodenheimer P., Burkert A., Klein R. I., Boss A. P., 2000, Protostars and Planets IV, p. 675

Bonnell I., Kroupa P., 1998, arXiv Astrophysics e-prints, pp arXiv:astro–ph/9802306

Boylan-Kolchin M., Springel V., White S. D. M., Jenkins A., Lemson G., 2009, Monthly Notices of the Royal Astronomical Society, 398, 1150

Breslau A., Steinhausen M., Vincke K., Pfalzner S., 2014, , 565, A130

Cabrit S., Pety J., Pesenti N., Dougados C., 2006, , 452, 897

Cai M. X., Kouwenhoven M. B. N., Portegies Zwart S. F., Spurzem R., 2017, , 470, 4337

Carmona A., et al., 2008, Astronomy and Astrophysics, 477, 839

Casertano S., Hut P., 1985, , 298, 80

Chevalier R. A., 2000, The Astrophysical Journal Letters, 538, L151

Chevance M., et al., 2020, arXiv:2004.06113 [astro-ph]

Christiaens V., Casassus S., Perez S., van der Plas G., Ménard F., 2014, , 785, L12

Clarke C. J., Pringle J. E., 1991, Monthly Notices of the Royal Astronomical Society, 249, 588

Clarke C. J., Pringle J. E., 1993, Monthly Notices of the Royal Astronomical Society, 261, 190

Clarke C. J., Bonnell I. A., Hillenbrand L. A., 2000, Protostars and Planets IV, p. 151

Close J. L., Pittard J. M., 2017, , 469, 1117

Dai F., Facchini S., Clarke C. J., Haworth T. J., 2015, , 449, 1996

Dinnbier F., Kroupa P., 2020, Astronomy and Astrophysics, 640, A84

Dobbs C. L., Liow K. Y., Rieder S., 2020, Monthly Notices of the Royal Astronomical Society, 496, L1

Dong R., Liu S.-y., Fung J., 2018, arXiv:1811.09629 [astro-ph]

Dunham M. M., et al., 2015, The Astrophysical Journal Supplement Series, 220, 11

Eisner J. A., Carpenter J. M., 2006, , 641, 1162

Eisner J. A., et al., 2018, , 860, 77

Elmegreen B. G., Efremov Y. N., 1997, The Astrophysical Journal, 480, 235

Elmegreen B. G., Falgarone E., 1996, The Astrophysical Journal, 471, 816

Elmegreen B. G., Scalo J., 2004, Annual Review of Astronomy and Astrophysics, 42, 211

Elmegreen B. G., Efremov Y., Pudritz R. E., Zinnecker H., 2000, Protostars and Planets IV, p. 179

Ercolano B., Clarke C. J., Hall A. C., 2011, Monthly Notices of the Royal Astronomical Society, 410, 671

Evans Neal J. I., et al., 2009, The Astrophysical Journal Supplement Series, 181, 321

Facchini S., Clarke C. J., Bisbas T. G., 2016, , 457, 3593

Facchini S., Birnstiel T., Bruderer S., Dishoeck E. F. v., 2017, , 605, A16

Falgarone E., Phillips T. G., 1991, 147, 119

Falgarone E., Phillips T. G., Walker C. K., 1991, The Astrophysical Journal, 378, 186

Fall S. M., Krumholz M. R., Matzner C. D., 2010, The Astrophysical Journal Letters, 710, L142

Fang M., et al., 2012, , 539, A119

Fatuzzo M., Adams F. C., 2008, , 675, 1361

Faucher-Giguère C.-A., Kaspi V. M., 2006, The Astrophysical Journal, 643, 332

Field G. B., Somerville W. B., Dressler K., 1966, Annual Review of Astronomy and Astrophysics, 4, 207

Field G. B., Blackman E. G., Keto E. R., 2008, Monthly Notices of the Royal Astronomical Society, 385, 181

Font A. S., McCarthy I. G., Johnstone D., Ballantyne D. R., 2004, , 607, 890

Forbes D. A., et al., 2018, Proceedings of the Royal Society A: Mathematical, Physical and Engineering Sciences, 474, 20170616

Francis L., van der Marel N., 2020, arXiv:2003.00079 [astro-ph]

Fujii M. S., Portegies Zwart S., 2011, Science, 334, 1380

Fujii M. S., Portegies Zwart S., 2015, , 449, 726

Fujii M. S., Portegies Zwart S., 2016, , 817, 4

Gieles M., Portegies Zwart S. F., 2011, Monthly Notices of the Royal Astronomical Society, 410, L6

Gnedin O. Y., Ostriker J. P., Tremaine S., 2014, The Astrophysical Journal, 785, 71

Goldsmith P. F., Bergin E. A., Lis D. C., 1997, The Astrophysical Journal, 491, 615

Goodwin S. P., 1997, Monthly Notices of the Royal Astronomical Society, 284, 785

Gorti U., Dullemond C. P., Hollenbach D., 2009, , 705, 1237–1251

Gorti U., Hollenbach D., Dullemond C. P., 2015, , 804, 29

Gounelle M., Meibom A., 2008, The Astrophysical Journal, 680, 781

Greaves J. S., Rice W. K. M., 2010, , 407, 1981

Grudić M. Y., Hopkins P. F., Faucher-Giguère C.-A., Quataert E., Murray N., Kereš D., 2018, Monthly Notices of the Royal Astronomical Society, 475, 3511

Guarcello M. G., Micela G., Damiani F., Peres G., Prisinzano L., Sciortino S., 2009, , 496, 453

Guarcello M. G., et al., 2016, arXiv:1605.01773 [astro-ph]

Gunn J. E., Gott J. Richard I., 1972, The Astrophysical Journal, 176, 1

Gutermuth R. A., et al., 2008, The Astrophysical Journal, 674, 336

Habing H. J., 1968, Bulletin of the Astronomical Institutes of the Netherlands, 19, 421

Hacar A., Tafalla M., Kauffmann J., Kovács A., 2013, Astronomy and Astrophysics, 554, A55

Haisch Karl E. J., Lada E. A., Lada C. J., 2001, , 553, L153

Hall S. M., Clarke C. J., Pringle J. E., 1996, Monthly Notices of the Royal Astronomical Society, 278, 303

Halley E., 1715, Philosophical Transactions of the Royal Society of London Series I, 29, 390

Hartmann L., Calvet N., Gullbring E., D'Alessio P., 1998, , 495, 385

Hartmann L., Herczeg G., Calvet N., 2016, Annual Review of Astronomy and Astrophysics, 54, 135

Haworth T. J., Facchini S., Clarke C. J., Mohanty S., 2018, , 475, 5460

Hernández J., et al., 2007, The Astrophysical Journal, 671, 1784

Hernquist L., Katz N., Weinberg D. H., Miralda-Escudé J., 1996, The Astrophysical Journal Letters, 457, L51

Hollenbach D., Johnstone D., Lizano S., Shu F., 1994, The Astrophysical Journal, 428, 654

Hoyle F., 1953, The Astrophysical Journal, 118, 513

Huang J., et al., 2020, arXiv:2001.11040 [astro-ph]

Hueso R., Guillot T., 2005, Astronomy and Astrophysics, 442, 703

Hunter C., 1964, The Astrophysical Journal, 139, 570

Hunter C., 1977, The Astrophysical Journal, 218, 834

Isella A., Carpenter J. M., Sargent A. I., 2009, , 701, 260

Isella A., Pérez L. M., Carpenter J. M., 2012, , 747, 136

Jeans J. H., 1902, Philosophical Transactions of the Royal Society of London Series A, 199, 1

Jílková L., Portegies Zwart S., Pijloo T., Hammer M., 2015, , 453, 3157

Johnstone D., Hollenbach D., Bally J., 1998, , 499, 758

Kant I., 1755, Zeitz, Bei W. Webel, 1798. Neue aufl.

Kim J. S., Clarke C. J., Fang M., Facchini S., 2016, , 826, L15

King I. R., 1966, The Astronomical Journal, 71, 64

Klessen R. S., Burkert A., 2000, The Astrophysical Journal Supplement Series, 128, 287

Klessen R. S., Burkert A., Bate M. R., 1998, The Astrophysical Journal Letters, 501, L205

Klessen R. S., Heitsch F., Mac Low M.-M., 2000, The Astrophysical Journal, 535, 887

Klypin A., Trujillo-Gomez S., Primack J., 2011, The Astrophysical Journal, 740, 102

Korycansky D. G., Papaloizou J. C. B., 1995, Monthly Notices of the Royal Astronomical Society, 274, 85

Kraus S., et al., 2020, arXiv:2004.01204 [astro-ph]

Krause M. G. H., et al., 2020, arXiv:2005.00801 [astro-ph]

Kruijssen J. M. D., 2009, Astronomy and Astrophysics, 507, 1409

Kruijssen J. M. D., 2014, Classical and Quantum Gravity, 31, 244006

Kruijssen J. M. D., Maschberger T., Moeckel N., Clarke C. J., Bastian N., Bonnell I. A., 2012, Monthly Notices of the Royal Astronomical Society, 419, 841

Krumholz M. R., Forbes J. C., 2015, Astronomy and Computing, 11, 1

Krumholz M. R., McKee C. F., 2020, Monthly Notices of the Royal Astronomical Society, 494, 624

Kuffmeier M., Goicovic F. G., Dullemond C. P., 2019, arXiv:1911.04833 [astro-ph]

Lada C. J., Lada E. A., 1991, 13, 3

Lada E. A., Lada C. J., 1995, The Astronomical Journal, 109, 1682

Lada C. J., Lada E. A., 2003, , 41, 57

Lada C. J., Margulis M., Dearborn D., 1984, The Astrophysical Journal, 285, 141

Lada E. A., Strom K. M., Myers P. C., 1993, pp 245–277

Lada C. J., et al., 2006, The Astronomical Journal, 131, 1574

Lamers H. J. G. L. M., Baumgardt H., Gieles M., 2010, Monthly Notices of the Royal Astronomical Society, 409, 305

Laplace P. S., 1796, Exposition du système du monde, by de Laplace, Pierre Simon, 1796.

Larson R. B., 1969, Monthly Notices of the Royal Astronomical Society, 145, 271

Larson R. B., 1985, Monthly Notices of the Royal Astronomical Society, 214, 379

Larson R. B., 1995, Monthly Notices of the Royal Astronomical Society, 272, 213

Larson R. B., 2003, Reports on Progress in Physics, 66, 1651

Longmore S. N., et al., 2014, Protostars and Planets VI, pp 291–314

Lucas W. E., Rybak M., Bonnell I. A., Gieles M., 2018, Monthly Notices of the Royal Astronomical Society, 474, 3582

Luhman K. L., Allen P. R., Espaillat C., Hartmann L., Calvet N., 2010, The Astrophysical Journal Supplement Series, 186, 111

Lynden-Bell D., Pringle J. E., 1974, , 168, 603

Madrid J. P., Leigh N. W. C., Hurley J. R., Giersz M., 2017, Monthly Notices of the Royal Astronomical Society, 470, 1729

Mamajek E. E., 2009,] 10.1063/1.3215910, 1158, 3

Manara C. F., Robberto M., Da Rio N., Lodato G., Hillenbrand L. A., Stassun K. G., Soderblom D. R., 2012, The Astrophysical Journal, 755, 154

Manara C. F., et al., 2016, Astronomy and Astrophysics, 591, L3

Manara C. F., Morbidelli A., Guillot T., 2018, , 618, L3

Mann R. K., Williams J. P., 2010, , 725, 430

Mann R. K., et al., 2014, , 784, 82

Marino S., et al., 2018, Monthly Notices of the Royal Astronomical Society, 479, 5423

Marino S., Yelverton B., Booth M., Faramaz V., Kennedy G. M., Matrà L., Wyatt M. C., 2019, Monthly Notices of the Royal Astronomical Society, 484, 1257

Masunaga H., Inutsuka S.-i., 2000, The Astrophysical Journal, 531, 350

Matzner C. D., 2002, The Astrophysical Journal, 566, 302

Matzner C. D., McKee C. F., 2000, The Astrophysical Journal, 545, 364

Mayor M., Queloz D., 1995, Nature, 378, 355

Menard F., et al., 2020, arXiv:2006.02439 [astro-ph]

Mestel L., 1965, Quarterly Journal of the Royal Astronomical Society, 6, 161

Mestel L., Spitzer L. J., 1956, Monthly Notices of the Royal Astronomical Society, 116, 503

Mitchell P. D., et al., 2017, arXiv:1709.08647 [astro-ph 10.1093/mnras/stx2770

Moeckel N., Throop H. B., 2009, The Astrophysical Journal, 707, 268

Mori M., Burkert A., 2000, The Astrophysical Journal, 538, 559

Mulders G. D., Dominik C., 2012, , 539, A9

Murray N., Rahman M., 2010, The Astrophysical Journal, 709, 424

Najita J. R., Kenyon S. J., 2014, , 445, 3315

Najita J. R., Andrews S. M., Muzerolle J., 2015, Monthly Notices of the Royal Astronomical Society, 450, 3559

Nakamura F., Li Z.-Y., 2012,] 10.1063/1.4754324, 1480, 30

Newton I., 1687, Newtoni principia philosophiæ. Apud Guil. & Joh. Innys, Regiæ Societatis typographos.

Nicholson R. B., Parker R. J., Church R. P., Davies M. B., Fearon N. M., Walton S. R. J., 2019,

O'dell C. R., 1998, , 115, 263

O'dell C. R., Wen Z., 1994, , 436, 194

Offner S. S. R., Arce H. G., 2015, The Astrophysical Journal, 811, 146

Offner S. S. R., Chaban J., 2017, The Astrophysical Journal, 847, 104

Owen J. E., Ercolano B., Clarke C. J., Alexander R. D., 2010, , 401, 1415

Owen J. E., Clarke C. J., Ercolano B., 2012, , 422, 1880

Paczynski B., 1977, The Astrophysical Journal, 216, 822

Pascucci I., et al., 2016, , 831, 125

Pelupessy F. I., Portegies Zwart S., 2012, , 420, 1503

Pelupessy F. I., van Elteren A., de Vries N., McMillan S. L. W., Drost N., Portegies Zwart S. F., 2013, , 557, A84

Pfalzner S., 2003, The Astrophysical Journal, 592, 986

Pfalzner S., Vogel P., Scharwächter J., Olczak C., 2005a, Astronomy and Astrophysics, 437, 967

Pfalzner S., Umbreit S., Henning T., 2005b, The Astrophysical Journal, 629, 526

Pfalzner S., Olczak C., Eckart A., 2006, , 454, 811

Pfalzner S., Bhandare A., Vincke K., Lacerda P., 2018, , 863, 45

Portegies Zwart S. F., 2016, , 457, 313

Portegies Zwart S. P., McMillan S., 2018, Astrophysical Recipes: The Art of AMUSE, 1st edn. AAS-IOP Astronomy, Institute of Physics Publishing, Great Britain

Portegies Zwart S., et al., 2009, *New Astronomy*, 14, 369

Portegies Zwart S. F., McMillan S. L. W., Gieles M., 2010, , 48, 431

Portegies Zwart S., McMillan S. L. W., van Elteren E., Pelupessy I., de Vries N., 2013, Computer Physics Communications, 183, 456

Portegies Zwart S., Pelupessy I., van Elteren A., Wijnen T. P. G., Lugaro M., 2018, , 616, A85

Prentice A. J. R., 1978, Moon and Planets, 19, 341

Pringle J. E., 1981, Annual Review of Astronomy and Astrophysics, 19, 137

Pringle J. E., 1989, Monthly Notices of the Royal Astronomical Society, 239, 361

Reche R., Beust H., Augereau J.-C., 2009, , 493, 661

Richling S., Yorke H. W., 1997, , 327, 317

Rodriguez J. E., et al., 2018, , 859, 150

Rosotti G. P., Dale J. E., de Juan Ovelar M., Hubber D. A., Kruijssen J. M. D., Ercolano B., Walch S., 2014, , 441, 2094

Russell S. S., Hartmann L., Cuzzi J., Krot A. N., Gounelle M., Weidenschilling S., 2006, Meteorites and the Early Solar System II, pp 233–251

Salyk C., Pontoppidan K., Corder S., Muñoz D., Zhang K., Blake G. A., 2014, , 792, 68

Scally A., Clarke C., 2001, , 325, 449

Scalo J., 1990,] 10.1007/978-94-009-0605-1-12, 162, 151

Scalo J., Elmegreen B. G., 2004, Annual Review of Astronomy and Astrophysics, 42, 275

Schaye J., et al., 2015, Monthly Notices of the Royal Astronomical Society, 446, 521

Shakura N. I., Sunyaev R. A., 1973, , 24, 337

Sicilia-Aguilar A., Hartmann L. W., Fürész G., Henning T., Dullemond C., Brandner W., 2006, , 132, 2135

Sicilia-Aguilar A., Henning T., Hartmann L. W., 2010, , 710, 597

Smith B. A., Terrile R. J., 1984, Science, 226, 1421

Spitzer Lyman J., 1940, Monthly Notices of the Royal Astronomical Society, 100, 396

Spitzer Lyman J., 1968, Nebulae and Interstellar Matter, p. 1

Spitzer L., 1987, Dynamical evolution of globular clusters

Springel V., Hernquist L., 2003, Monthly Notices of the Royal Astronomical Society, 339, 289

Springel V., et al., 2005, Nature, 435, 629

Spurzem R., Giersz M., Heggie D. C., Lin D. N. C., 2009, The Astrophysical Journal, 697, 458

Störzer H., Hollenbach D., 1999, , 515, 669

Strom K. M., Strom S. E., Edwards S., Cabrit S., Skrutskie M. F., 1989, The Astronomical Journal, 97, 1451

Sung H., Stauffer J. R., Bessell M. S., 2009, The Astronomical Journal, 138, 1116

Takahashi K., Portegies Zwart S. F., 2000, The Astrophysical Journal, 535, 759

Torres S., Cai M. X., Brown A. G. A., Portegies Zwart S., 2019, Astronomy and Astrophysics, 629, A139

Trapman L., Facchini S., Hogerheijde M. R., van Dishoeck E. F., Bruderer S., 2019, , 629, A79

Trapman L., Rosotti G., Bosman A. D., Hogerheijde M. R., van Dishoeck E. F., 2020, arXiv:2005.11330 [astro-ph]

Trumpler R. J., 1930, Leaflet of the Astronomical Society of the Pacific, 1, 117

Tychoniec , et al., 2020, arXiv:2006.02812 [astro-ph]

Vázquez-Semadeni E., Palau A., Ballesteros-Paredes J., Gómez G. C., Zamora-Avilés M., 2019, Monthly Notices of the Royal Astronomical Society, 490, 3061

Vicente S. M., Alves J., 2005, , 441, 195

Vincke K., Pfalzner S., 2016, , 828, 48

Vincke K., Breslau A., Pfalzner S., 2015, , 577, A115

Vink J. S., de Koter A., Lamers H. J. G. L. M., 2001, Astronomy and Astrophysics, 369, 574

Wijnen T. P. G., Pols O. R., Pelupessy F. I., Portegies Zwart S., 2016, , 594, A30

Wijnen T. P. G., Pols O. R., Pelupessy F. I., Portegies Zwart S., 2017a, , 602, A52

Wijnen T. P. G., Pols O. R., Pelupessy F. I., Portegies Zwart S., 2017b, Astronomy and Astrophysics, 604, A91

Williams J. P., 2012, Meteoritics and Planetary Science, 47, 1915

Williams J. P., Cieza L. A., 2011, , 49, 67

Williams J. P., McKee C. F., 1997, The Astrophysical Journal, 476, 166

Williams J. P., Blitz L., McKee C. F., 2000, Protostars and Planets IV, p. 97

Williams J. P., Cieza L., Hales A., Ansdell M., Ruiz-Rodriguez D., Casassus S., Perez S., Zurlo A., 2019, arXiv:1904.06471 [astro-ph]

Winkler K.-H. A., Newman M. J., 1980, The Astrophysical Journal, 236, 201

Winston E., et al., 2007, The Astrophysical Journal, 669, 493

Winter A. J., Clarke C. J., Rosotti G., Booth R. A., 2018a, , 475, 2314

Winter A. J., Clarke C. J., Rosotti G., Ih J., Facchini S., Haworth T. J., 2018b, , 478, 2700

Winter A. J., Booth R. A., Clarke C. J., 2018c, , 479, 5522

Winter A. J., Clarke C. J., Rosotti G. P., 2019, , 485, 1489

Winter A. J., Kruijssen J. M. D., Chevance M., Keller B. W., Longmore S. N., 2020, , 491, 903

Wuchterl G., Tscharnuter W. M., 2003,] 10.1051/0004-6361:20021707, 398, 1081

Yorke H. W., Bodenheimer P., Laughlin G., 1993, The Astrophysical Journal, 411, 274

de Juan Ovelar M., Kruijssen J. M. D., Bressert E., Testi L., Bastian N., Cánovas H., 2012, , 546, L1

van Boekel R., et al., 2017, The Astrophysical Journal, 837, 132

van Elteren A., Portegies Zwart S., Pelupessy I., Cai M. X., McMillan S. L. W., 2019, , 624, A120

van Terwisga S. E., et al., 2020, arXiv:2004.13551 [astro-ph]

van der Marel N., Matthews B., Dong R., Birnstiel T., Isella A., 2018, arXiv:1809.06403 [astro-ph]